Synthesis and Characterization of the Dimethyl-Substituted Bisbenzimidazole Ligand and Its Manganese Complex

Wai Him Kwok,[†,‡] Huichang Zhang,[†,‡] Pramatha Payra,[†,‡] Maosheng Duan,[†,‡] Shao-ching Hung,[§,‡] Dean H. Johnston,[∥] Judith Gallucci,[†] Ewa Skrzypczak-Jankun,[⊥] and Michael K. Chan*[,†]

Departments of Chemistry and Biochemistry, The Ohio State University, 100 West 18th Avenue, Columbus, Ohio 43210, Department of Chemistry, California Institute of Technology, Pasadena, California 91734, Department of Chemistry, Otterbein College, Westerville, Ohio 43081, and Department of Chemistry, The University of Toledo, Toledo, Ohio 43606

Received November 15, 1999

Macrocycles with unique properties provide new avenues for the design of novel catalysts and materials. Here, we report, for the first time, the synthesis and characterization of the dimethyl-substituted bisbenzimidazole ligand (Me_2BBZ) and its manganese complex ($Mn-Me_2BBZ$). The Me_2BBZ ligand is similar to porphyrin and phthalocyanine macrocycles in terms of its cavity size and metal-binding mode, but owing to electronic and charge differences, it exhibits properties that make it distinct from its structural counterparts. For instance, the optical spectra of bisbenzimidazoles lack transitions in the 500−900 nm region. Perhaps the most significant feature of the Me_2BBZ ligand, however, is its inherent nonplanarity. Geometric restraints within this nonplanar ligand give rise to two atropisomers, which, when separated, could have potential in chiral catalysis and recognition. In addition, here we show that this nonplanarity can help to promote unusual crystal-packing interactions. Within the structure of the $Mn-Me_2BBZ$ complex, intermolecular π-stacking interactions of the phenyl and benzimidazole groups lead to the formation of a distinct two-dimensional "staircase" lattice comprised of alternating $Mn-Me_2BBZ$ atropisomers. The potential significance of this structural arrangement is revealed by temperature-dependent magnetic studies that indicate weak antiferromagnetic coupling between the metal ions in the crystal. Fine-tuning of these long-range electronic and magnetic interactions could be useful for the design of novel molecular materials.

In nature, metallotetrapyrrole cofactors (hemes, corrins, F430) facilitate the sensing,[1−5] transport,[6,7] and catalysis[8−14] of important biomolecules. Synthetic models of these cofactors have found use in numerous applications as well, including the catalytic oxidation of organic substrates[15−20] and the fabrication of novel materials.[21−23] In light of the general importance of these compounds, the study of tetrapyrroles and their related metal complexes has remained an active area of research despite extensive investigation.[15,20,24−28]

As a new direction in the study of tetrapyrrole analogues, we have endeavored to develop a new class of "bisbenzimid-

* To whom correspondence should be addressed. Telephone: 614-292-8375. Fax: 614-292-6773. E-mail: chan@chemistry.ohio-state.edu.
† The Ohio State University.
‡ The first five authors contributed equally to the project.
§ California Institute of Technology.
∥ Otterbein College.
⊥ The University of Toledo.

(1) Gong, W.; Hao, B.; Mansy, S. S.; Gonzalez, G.; Gilles-Gonzalez, M. A.; Chan, M. K. *Proc. Natl. Acad. Sci. U.S.A.* **1998**, *95*, 15177−15182.
(2) Gilles-Gonzalez, M. A.; Ditta, G.; Helinski, D. R. *Nature* **1991**, *350*, 170−172.
(3) Gilles-Gonzalez, M. A.; Gonzalez, G.; Perutz, M. F.; Kiger, L.; Marden, M.; Poyart, C. *Biochemistry* **1994**, *33*, 8067−8073.
(4) Garbers, D. L.; Lowe, D. G. *J. Biol. Chem.* **1994**, *269*, 30741−30744.
(5) Shelver, D.; Kerby, R. L.; He, Y.; Roberts, G. P. *Proc. Natl. Acad. Sci. U.S.A.* **1997**, *94*, 11216−11220.
(6) Perutz, M. F. *Nature* **1970**, *228*, 726−739.
(7) Weichsel, A.; Anderson, J. F.; Champagne, D. E.; Walker, F. A.; Montfort, W. R. *Nature Struct. Biol.* **1998**, *5*, 304−309.
(8) Ludwig, M. L.; Drennan, C. L.; Matthews, R. G. *Structure* **1996**, *4*, 505−512.
(9) Ludwig, M. L.; Matthews, R. G. *Annu. Rev. Biochem.* **1997**, *66*, 269−313.
(10) Drennan, C. L.; Matthews, R. G.; Ludwig, M. L. *Curr. Opin. Struct. Biol.* **1994**, *4*, 919−29.
(11) Drennan, C. L.; Huang, S.; Drummond, J. T.; Matthews, R. G.; Ludwig, M. *Science* **1994**, *266*, 1669−1674.
(12) Furenlid, L. R.; Renner, M. W.; Fajer, J. *J. Am. Chem. Soc.* **1990**, *112*, 8987−8989.
(13) Ermler, U.; Grabarse, W.; Shima, S.; Goubeaud, M.; Thauer, R. K. *Science* **1997**, *278*, 1413−1415.
(14) Sono, M.; Roach, M. P.; Coulter, E. D.; Dawson, J. H. *Chem. Rev.* **1996**, *96*, 2841−88.
(15) Meunier, B. *Chem. Rev.* **1992**, *21*, 1411−1456.
(16) Groves, J. T.; Myers, R. S. *J. Am. Chem. Soc.* **1983**, *105*, 5791−5796.
(17) Groves, J. T.; Takahashi, T. *J. Am. Chem. Soc.* **1983**, *105*, 2073−2074.
(18) Groves, J. T.; Viski, P. *J. Am. Chem. Soc.* **1989**, *111*, 8537−8538.
(19) Groves, J. T.; Viski, P. *J. Org. Chem.* **1990**, *55*, 3628−3634.
(20) Collman, J. P.; Zhang, X.; Lee, V. J.; Uffelman, E. S.; Brauman, J. I. *Science* **1993**, *261*, 1404−1411.
(21) Moser, F. H.; Thomas, A. L. *The Phthalocyanines: Manufacture and Applications*; CRC Press: Boca Raton, FL, 1983; Vol. 2.
(22) Akerfeldt, K. S.; Kim, R. M.; Camac, D.; Groves, J. T.; Lear, J. D.; DeGrado, W. F. *J. Am. Chem. Soc.* **1992**, *114*, 9656−9657.
(23) Drain, C. M.; Nifiatis, F.; Vasenko, A.; Batteas, J. D. *Angew. Chem., Int. Ed. Engl.* **1998**, *37*, 2344−2347.
(24) Sessler, J. L. *Expanded, contracted & isomeric porphyrins*; Pergamon: Oxford, U.K., 1997; Vol. 15.
(25) Gale, P. A.; Sessler, J. L.; Král, V. *Chem. Commun.* **1998**, 1−8.
(26) Velazquez, C. S.; Broderick, W. E.; Sabat, M.; Barrett, A. G. M.; Hoffman, B. M. *J. Am. Chem. Soc.* **1990**, *112*, 7408−7410.
(27) Strachan, J.-P.; Gentemann, S.; Seth, J.; Kalsbeck, W. A.; Lindsey, J. S.; Holten, D.; Bocian, D. F. *J. Am. Chem. Soc.* **1997**, *119*, 11191−11201.
(28) Drain, C. M.; Lehn, J.-M. *J. Chem. Soc., Chem. Commun.* **1994**, 2313−2315.

10.1021/ic991322a CCC: $19.00 © 2000 American Chemical Society
Published on Web 05/03/2000

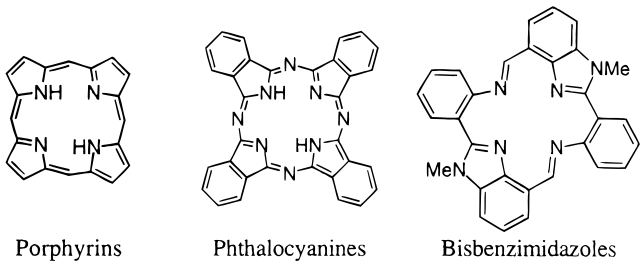

Figure 1. Comparison of porphyrins, phthalocyanines, and bisbenzimidazoles.

azole" ligand based on aminophenylbenzimidazole units (see Figure 1). This macrocycle has the same ring size as a porphyrin or phthalocyanine, suggesting that it might exhibit similar metal-chelating behavior. Unlike these classical tetrapyrroles, however, molecular mechanics calculations (HYPERCHEM, version 4.5, Hypercube Inc.) predict that bisbenzimidazole complexes should be inherently nonplanar. In light of the fact that this nonplanarity leads to two distinct hands, bisbenzimidazole complexes may have potential for promoting the chiral recognition of ligands and substrates. In addition, bisbenzimidazole ligands offer potential synthetic advantages over porphyrins. Because of the ease of substitution at the N-3 benzimidazole nitrogen, the preparation of derivatized forms is relatively straightforward.

Here, we describe a convenient approach toward the synthesis of the dimethyl-substituted bisbenzimidazole (Me_2BBZ) ligand shown in Figure 1. Various metal complexes with this new ligand have been prepared, and their optical, electrochemical, and magnetic properties have been characterized. In this first report, we summarize the results that have been obtained for the diprotonated ligand and its manganese complex. These studies reveal distinct differences between bisbenzimidazoles and classical tetrapyrroles.

Experimental Section

^{1}H NMR spectra were recorded on a Bruker WM 200 (200 MHz) spectrometer. Spectra were referenced internally to the residual proton resonance of $CDCl_3$ (δ, 7.26 ppm) as the internal standard. Chemical shifts (δ) are reported as part per million (ppm) on the δ scale. Coupling constants (J) are reported in hertz (Hz). NMR spectroscopic terms are reported by using the following abbreviations: s, single; d, doublet; t, triplet; m, multiplet.

Unless otherwise noted, all materials were obtained from commercial suppliers and used without further purification. Thin-layer chromatography was performed on Whatman precoated silica gel UV_{254} plates. Silica gel (Scientific Adsorbents Inc. 32-63 U, 40 μm) was used for column chromatography.

2,3-Diaminobenzyl Alcohol (2). Raney nickel (~5 g) was placed in a hydrogenation bottle and washed with THF three times before being slurried in 50 mL of THF. 4-Hydroxymethyl-2,1,3-benzothiadiazole[29] (5.0 g, 30 mmol) was then added. It was hydrogenated under 10 psi pressure at room temperature for 6 h. TLC was used to confirm that all starting material had been consumed. The resulting reaction mixture was filtered carefully through a pad of Celite and washed with THF. After removal of the solvent, 2,3-diaminobenzyl alcohol (4.0 g, 96%) was obtained as a colorless crystalline solid. R_f = 0.18 (hexane/ethyl acetate/MeOH = 5:5:1). ^{1}H NMR (200 MHz, DMSO): δ 4.33 (broad s, 2 H), 4.36 (d, J = 5.4 Hz, 2 H), 4.43 (broad s, 2 H), 4.96 (t, J = 5.4 Hz, 1 H), 6.43 (m, 3 H). HRMS: Calcd for $C_7H_{10}N_2O$, 138.0793; found, 138.0830.

4-Hydroxymethyl-2-(2-nitrophenyl)benzimidazole (3). 2,3-Diaminobenzyl alcohol **2** (3.45 g, 25 mmol) was dissolved in a MeOH/H_2O mixture (200 mL, v/v = 1:1). Acetic acid (3 mL), 2-nitrobenzaldehyde (5.3 g, 35 mmol) in MeOH (50 mL), and $Cu(OAc)_2 \cdot H_2O$ (7.0 g, 35 mmol) in water (100 mL) were added sequentially to the stirring solution. It was then heated to reflux under vigorous stirring for 3 h, after which a pale-yellow precipitate was formed. The mixture was filtered hot and then washed with water to afford a gray-yellow solid. The precipitate was redissolved in EtOH (150 mL) and concentrated HCl (24 mL), and then a solution of $Na_2S \cdot 9H_2O$ (12.8 g, 50 mmol) in water (100 mL) was added. The mixture was heated at reflux for 1 h, resulting in a black slurry. It was then allowed to cool to room temperature and filtered through a pad of Celite to remove the precipitated CuS. The filtrate was neutralized with ammonium hydroxide to pH = 8−9 and then concentrated by rotary evaporation to yield a green-yellow precipitate. After filtration and vacuum evaporation, 4-hydroxymethyl-2-(2-nitrophenyl)benzimidazole (5.55 g, 82%) was obtained as a green-yellow solid. R_f = 0.28 (hexane/ethyl acetate = 1:2). ^{1}H NMR (200 MHz, DMSO): δ 4.84 (broad s, 2 H), 5.22 (broad s, 1 H), 7.28 (m, 2 H), 7.49 (d, J = 6.8 Hz, 1 H), 7.71−8.06 (m, 4 H), 12.93 (broad s, 1 H). HRMS: Calcd for $C_{14}H_{11}N_3O_3$, 269.0800; found, 269.0845.

2-(2-Nitrophenyl)benzimidazole-4-carboxaldehyde (4). 4-Hydroxymethyl-2-(2-nitrophenyl)benzimidazole (**3**) (2.69 g, 10 mmol) was dissolved in a mixture of CH_3CN/CH_2Cl_2 (500 mL, v/v = 4:1), and then manganese dioxide (10 g, 120 mmol) was added. The solution was stirred at room temperature and monitored by TLC. Once the reaction was complete, the reaction mixture was filtered through a pad of Celite. The filtrate was washed with $NaHCO_3$, and the water phase was extracted with CH_2Cl_2. The combined organic layer was washed with brine and dried over Na_2SO_4. Concentration by rotary evaporation and subsequent column chromatography on silica gel using hexane/ethyl acetate (1:1) as the eluent afforded 2-(2-nitrophenyl)benzimidazole-4-carboxaldehyde (2.2 g, 82%) as a light-yellow solid. R_f = 0.38 (hexane/ethyl acetate = 1:1). ^{1}H NMR (200 MHz, $CDCl_3$): δ 7.47 (t, J = 7.6 Hz, 1 H), 7.63−7.82 (m, 3 H), 7.94 (d, J_1 = 7.5 Hz, J_2 = 1.5 Hz, 1 H), 8.05 (d, J_1 = 7.7 Hz, J_2 = 1.6 Hz, 1 H), 8.10 (d, J = 8.1 Hz, 1 H), 10.11 (s, 1 H), 11.21 (broad s, 1 H). HRMS: Calcd for $C_{14}H_9N_3O_3$, 267.0644; found, 267.0648.

2-(2-Nitrophenyl)benzimidazole-4-carboxaldehyde Ethylene Acetal (5). 2-(2-Nitrophenyl)benzimidazole-4-carboxaldehyde (**4**) (6.27 g, 23.5 mmol) was dissolved in benzene (150 mL) and mixed with ethylene glycol (6.5 mL, 118 mmol) and *p*-toluenesulfonic acid monohydrate (0.450 g, 2.35 mmol). The mixture was heated to reflux overnight, and the water was removed by azeotropic distillation. The resulting solution was allowed to cool to room temperature and was then neutralized with saturated $NaHCO_3$, washed with water and brine, and dried over Na_2SO_4. The compound was purified by column chromatography on silica gel using hexane/ethyl acetate (1:2) as the eluent to give 2-(2-nitrophenyl)benzimidazole-4-carboxaldehyde ethylene acetal (4.552 g, 62.2%) as a yellow solid. R_f = 0.24 (hexane/ethyl acetate = 1:2). ^{1}H NMR (200 MHz, $CDCl_3$): δ 4.11 (m, 2 H), 4.20 (m, 2 H), 6.15 (s, 1H), 7.30 (m, 2 H), 7.57−7.83 (m, 3 H), 7.93 (d, J_1 = 7.8 Hz, J_2 = 1.3 Hz, 1 H), 8.13 (d, J_1 = 7.7 Hz, J_2 = 1.5 Hz, 1 H), 10.48 (broad s, 1 H). HRMS: Calcd for $C_{16}H_{13}N_3O_4$, 311.0906; found, 311.0915.

1-Methyl-2-(2-nitrophenyl)benzimidazole-4-carboxaldehyde Ethylene Acetal (6). A solution of 2-(2-nitrophenyl)benzimidazole-4-carboxaldehyde ethylene acetal (**5**) (4.53 g, 14.6 mmol) in dry THF (20 mL) was added to a stirring suspension of NaH (0.640 g, 60% dispersion in mineral oil, 16.0 mmol) in dry THF (50 mL) at 0 °C under N_2. The mixture was then allowed to warm to room temperature for 1 h, resulting in an orange solution. Methyl iodide (4.58 mL, 72.8 mmol) was syringed into the above mixture at room temperature under N_2. This mixture was stirred for 24 h under N_2 to give a yellow solution. Water was added, and the aqueous layer was extracted with $CHCl_3$. The combined extracts were washed with brine and dried over Na_2SO_4. After rotary evaporation, the resulting residue was purified by column chromatography on silica gel using Et_2O/CH_2Cl_2 (3:1) as the eluent to give the title compound (3.53 g, 74%). ^{1}H NMR ($CDCl_3$): δ 3.58 (s, 3 H), 4.02−4.19 (m, 4 H), 6.55 (s, 1 H), 7.33−7.41 (m, 1 H), 7.52−7.56 (m, 1 H), 7.62−7.75 (m, 4 H), 8.19 (d, J = 1.7, 7.9 Hz, 1 H). HRMS: Calcd for $C_{17}H_{15}N_3O_4$, 325.1062; found, 325.1050.

(29) Jonas, R.; Prücher, H.; Wurziger, H. *Eur. J. Med. Chem.* **1993**, *28*, 141−148.

1-Methyl-2-(2-aminophenyl)benzimidazole-4-carboxaldehyde Ethylene Acetal (7). A solution of **6** (0.85 g, 2.6 mmol) in 50 mL of MeOH was mixed with 85 mg of Pd/C and hydrogenated with H_2 at a pressure of 10 psi for 3 h. The mixture was then filtered, and the solvent was removed to give 0.76 g (98%) of the title compound as a white solid. ^{1}H NMR ($CDCl_3$): δ 4.44 (s, 3 H), 4.69−4.90 (m, 4 H), 5.69 (broad s, 2 H), 7.44 (d, J = 7.8 Hz, 2 H), 7.81−8.05 (m, 4 H), 8.14 (d, J = 1.6, 6.9 Hz, 1 H). HRMS: Calcd for $C_{17}H_{17}N_3O_2$, 295.1321; found, 295.1325.

[H_2(Me_2BBZ)](ClO_4)$_2$ (8). 1-Methyl-2-(2-aminophenyl)benzimidazole-4-carboxaldehyde ethylene acetal (**7**) (0.62 g, 2.1 mmol) was dissolved in CH_3CN (15 mL) at room temperature, and then perchloric acid (0.42 mL, 2.3 mmol) was added. The mixture was stirred at room temperature for 2 days to yield a white suspension. It was then filtered to give the title compound as a white powder (0.56 g, 80%). ^{1}H NMR (DMSO): δ 4.06 (s, 6 H), 7.63−7.73 (m, 6 H), 7.81 (t, J = 8.0 Hz, 2 H), 7.94 (t, J = 7.6 Hz, 2 H), 8.04 (d, J = 7.4 Hz, 2 H), 8.10 (d, J = 7.2 Hz, 2 H), 8.26 (d, J = 8.2 Hz, 2 H), 8.94 (s, 2 H). Crystals suitable for X-ray analysis were obtained from recrystallization from CH_3CN. Anal. Calcd for [H_2(Me_2BBZ)](ClO_4)$_2$: C, 53.97; H, 3.59; N, 12.59; Cl, 10.64. Found: C, 53.94; H, 3.63; N, 12.66; Cl, 10.63.

Synthesis of [Mn(Me_2BBZ)Cl]Cl (9). Perchloric acid (0.185 mL, 2.15 mmol) was added to a solution of **7** (0.634 g, 2.15 mmol) in CH_3CN. The resulting pale-yellow solution was stirred for 20 h. Et_3N (0.5 mL, 13.6 mmol) was then added to form a yellow suspension that was stirred for 2 h, at which point, the solvent was removed by rotary evaporation. The product was triturated with water, filtered and washed with CH_3CN, and then dried at room temperature to give the free Me_2BBZ ligand as a pale-yellow solid (0.45 g, 90%). HRMS: Calcd for $C_{30}H_{22}N_6$, 466.1906; found, 466.1914.

The [Mn(Me_2BBZ)Cl]Cl complex (**9**) was prepared by refluxing the unpurified free Me_2BBZ ligand (0.497 g, 0.92 mmol) with $MnCl_2\cdot 4H_2O$ (0.1824 g, 0.92 mmol) in CH_3CN. An orange mixture was obtained upon stirring. The solution was refluxed for 20 h, and then the solvent was removed by rotary evaporation. The crude product was purified by column chromatography (CH_2Cl_2/hexane/MeOH = 3:1:1) (R_f = 0.73) and then dried to give an orange solid (0.45 g, 82% yield). Crystals of the [Mn(Me_2BBZ)Cl]Cl complex suitable for X-ray analysis were obtain by evaporation from CH_3CN. Anal. Calcd for [Mn(Me_2BBZ)Cl]Cl·$4H_2O$: C, 59.03; H, 3.93; N, 13.77; Cl, 11.62. Found: C, 57.97; H, 3.84; N, 13.39; Cl, 12.27.

Structure Determination/Refinement. (a) Structure of [H_2(Me_2BBZ)](ClO_4)$_2$. The data collection crystal was a yellow plate. Data were collected on a Siemens SMART diffractometer with a CCD area detector (Siemens CCD 1K) at the University of Toledo's Instrumentation Center. Examination of the diffraction pattern indicated a monoclinic system. Unit cell constants were obtained by a least-squares fit for 6397 reflections using graphite monochromated Mo Kα radiation (λ = 0.710 73 Å). A full sphere of data was collected, and data integration was done with the SAINT software (version 5.0, Bruker Analytic X-ray Systems). The data were 88% complete to 2θ = 55°. An absorption correction was applied to the data with the SADABS program,[30] with the maximum and minimum effective transmission factors of 1.0 and 0.797, respectively. Averaging the symmetry-equivalent reflections resulted in an R_{int} value of 0.056.

The structure was solved by direct methods in SHELXS-86.[31] Full-matrix least-squares refinements based on F^2 were performed in SHELXL-93.[32] While both perchlorate groups had large displacement parameters for the oxygen atoms, one group was better behaved than the other. An attempt was made to model the disorder in the perchlorate containing Cl(2). There appears to be a second orientation for this group that can be obtained by rotating about the Cl(2)−O(5) bond. The occupancy factors for O(6), O(7), and O(8) were each set at 0.65, while those for O(6A), O(7A), and O(8A) were set at 0.35. Cl(2) and O(5) were refined anisotropically, while the disordered oxygen atoms were refined isotropically. O(8A) acquired a very large U value, while all the other oxygen atoms refined to fairly reasonable U values. As a result, O(8A) was removed from the model.

The hydrogen atoms were included in the model at calculated positions using a riding model with $U(H) = 1.2U_{eq}$(attached carbon atom). For a methyl group, the torsion angle that defines its orientation was allowed to refine, and these hydrogen atoms were assigned to $U(H) = 1.5U_{eq}$(attached carbon atom). The final refinement cycle was based on all the 6703 intensities and 410 variables and resulted in agreement factors of $R_1(F)$ = 0.169 and wR2(F^2) = 0.258. For the subset of data with $I > 2\sigma(I)$ the $R_1(F)$ value is 0.097 (for 3768 reflections). The large R factors result from the disordered perchlorate group and the weak intensities of the overall data set. The final difference electron density map contains maximum and minimum peak heights of 1.01 and −0.92 e/Å^3, respectively. The maximum peak is in the vicinity of the disordered perchlorate ion. Neutral atom scattering factors were used and include terms for anomalous dispersion.[33]

(b) Structure of [Mn(Me_2BBZ)Cl]Cl. The data collection crystal was an orange-red irregular plate. Data were collected on a Siemens SMART diffractometer with a CCD area detector (Siemens CCD 1K) at the University of Toledo's Instrumentation Center. Examination of the diffraction pattern indicated a triclinic crystal system. Unit cell constants were obtained by a least-squares fit for 3807 reflections using graphite monochromated Mo Kα radiation (λ = 0.710 73 Å). A full sphere of data were collected using the ω scan method with narrow frames of 0.3°. Data integration was done with the SAINT software (version 5.0, Bruker Analytic X-ray Systems). The data are 89.2% complete to 2θ = 60 and 98.6% complete to 2θ = 55°. An absorption correction was applied to the data with the SADABS program,[30] with the maximum and minimum effective transmission factors of 1.0 and 0.822, respectively. Averaging the symmetry-equivalent reflections resulted in an R_{int} value of 0.049.

The structure was solved by the Patterson method using SHELXS-86[31] in $P\bar{1}$. Full-matrix least-squares refinements based on F^2 were performed in SHELXL-93.[32] The Mn complex packs in such a manner that channels are formed that run along the a-axis direction and are centered at $y = z = 0$. The Cl^- ion resides in this channel along with some disordered water molecules. Because it was difficult to obtain a satisfactory model of the water molecules within this channel, the density in the channel was accounted for using the SQUEEZE program[34] of PLATON.[35] This program modifies the observed structure factors by subtracting contributions from them on the basis of the electron density in the channel. In this case, the contributions of all of the electron density in the channel, including the Cl^- ion, were subtracted from the observed structure factors. (This is the reason no positional coordinates for the Cl^- ion appear in the table of atomic coordinates in the Supporting Information.) This channel region occupies 244 Å^3 per unit cell, and the electron density removed by this SQUEEZE procedure amounts to 41 electrons/unit cell. This corresponds to two Cl^- anions and one water molecule per unit cell.

The hydrogen atoms were included in the model at calculated positions using a riding model with $U(H) = 1.2U_{eq}$(attached carbon atom). For a methyl group, the torsion angle that defines its orientation was allowed to refine, and these hydrogen atoms were assigned to $U(H) = 1.5U_{eq}$(attached carbon atom). The (0 2 2) reflection was omitted from the final refinements because it had a significantly larger $\Delta(F^2)$/esd value than the other reflections. The final refinement cycle was based on all 7289 intensities and 345 variables and resulted in agreement factors of $R_1(F)$ = 0.128 and wR2(F^2) = 0.120. For the subset of data with $I > 2\sigma(I)$ the $R_1(F)$ value is 0.051 (for 3638 reflections). The final difference electron density map contains maximum and minimum peak heights of 0.23 and −0.23 e/Å^3. Neutral atom scattering factors were used and include terms for anomalous dispersion.[33]

X-band EPR Spectra of the Mn−Me_2BBZ Complex. A 5 mg/mL sample of the Mn−Me_2BBZ complex was dissolved in methanol/ethanol solution and frozen under liquid nitrogen to obtain a suitable

(30) Sheldrick, G. M. *SADABS*; University of Göttingen: Göttingen, Germany, 1997.
(31) Sheldrick, G. M. *Acta Crystallogr.* **1990**, *A46*, 467−473.
(32) Sheldrick, G. M. *SHELXL-93, Program for the Refinement of Crystal Structures*; University of Göttingen: Göttingen, Germany, 1993.
(33) *International Tables for Crystallography*; Kluwer Academic Publishers: Dordrecht, The Netherlands, 1992; Vol. C.
(34) van der Sluis, P.; Spek, A. L. *Acta Crystallogr.* **1990**, *A46*, 194−201.
(35) Spek, A. L. *Acta Crystallogr.* **1990**, *A46*, C-34.

Scheme 1

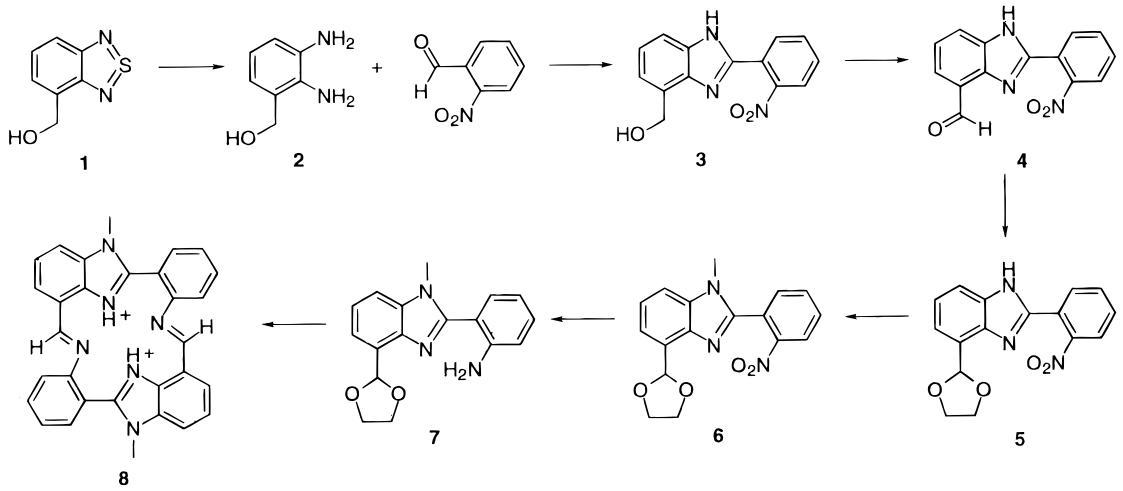

glass. The EPR experiments were performed on a Varian E-109 X-band spectrometer equipped with a E-231 TE-102 rectangular cavity and interfaced to an IBM personal computer for accumulation and digitization of the spectra. The sample temperature was controlled by variable temperature helium flow cryostat system (Oxford Instruments). EPR spectra of the compound were taken at several temperatures: 4.2, 10, 30, 50, 77, 173, and 200 K.

Temperature-Dependent Magnetization Measurements of the Mn−Me$_2$BBZ Complex. Field- and temperature-dependent magnetization measurements were performed on a Quantum Design MPMS superconducting quantum interference device (SQUID) magnetometer. Samples were held in either gel capsule or delrin screw-cap holders. The diamagnetic correction of the sample and holder, χ_{dia}, was determined from a plot of the measured magnetic susceptibility, χ_{obs}, vs inverse temperature. The correction was estimated from the intercept upon extrapolation to infinite temperature. The magnetization of the sample was measured between 0 and 55 kG at constant temperature (1.9 K). The variable temperature behavior was determined between 2 and 300 K at constant field (500 G). The data were fitted to the Curie−Weiss law, $\chi_m = C/(T - \theta)$, where χ_m is the molar magnetic susceptibility. θ has the units of temperature (K) and was obtained empirically from a plot of χ_m^{-1} vs T. The spin of the system (S) was calculated from the susceptibility ($\chi_m = Ng^2\mu_B^2S(S+1)/(3kT) = N\mu_{eff}^2/(3kT)$).

Results

Ligand Synthesis. A number of strategies were explored for the synthesis of the dimethyl-substituted bisbenzimidazole macrocycle. One successful route is shown in Scheme 1. The precursor 4-hydroxymethyl-2,1,3-benzothiadiazole (**1**),[29] was reduced with Raney nickel to yield 2,3-diaminobenzyl alcohol (**2**). The phenylbenzimidazole backbone was formed by the condensation of **2** with 2-nitrophenyl-1-carboxaldehyde using copper acetate coupling conditions,[36] yielding compound **3**. The benzyl group of **3** was allowed to oxidize to the corresponding aldehyde, **4**, in the presence of manganese dioxide and then converted to the acetal, **5**, by reaction with ethylene glycol. With the aldehyde and amine functionalities masked as acetal and nitro groups, respectively, incorporation of a methyl group at the N-3 benzimidazole nitrogen could be achieved by treatment of **5** with methyl iodide in the presence of sodium hydride, yielding **6**. Reduction of the nitro group of **6** with hydrogen, catalyzed by Pd on carbon, followed by the addition of perchloric acid unmasked both the amine and carboxaldehyde functionalities. Dimerization and cyclization of the resulting phenylbenzimidazole precursor gave the desired Me$_2$BBZ ligand.

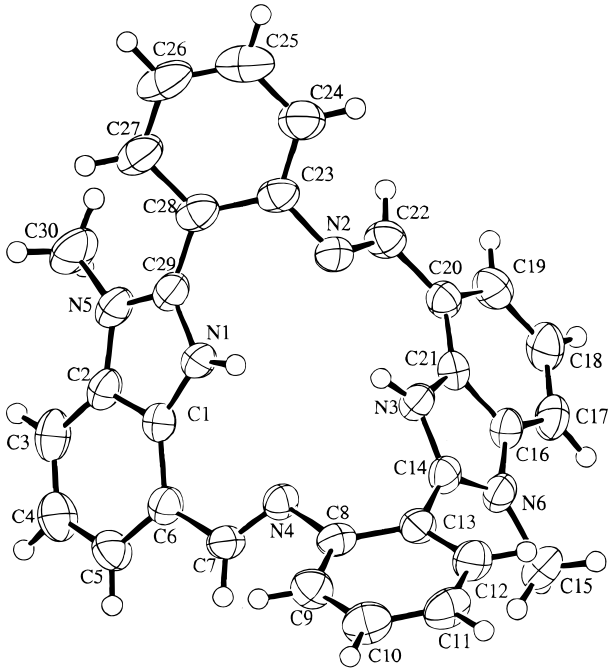

Figure 2. ORTEP diagram of $[H_2(Me_2BBZ)](ClO_4)_2$ (**8**).

Structural Studies. The correct identity of the Me$_2$BBZ ligand was confirmed by the crystal structure of its diprotonated form shown in Figure 2 (see Tables 1 and 2). The structure shows that, as expected, the benzimidazole framework is methylated on the outer benzimidazole nitrogens, N(5) and N(6), and that protonation occurs on the inner benzimidazole nitrogens, N(1) and N(3). Perhaps the most interesting feature of this structure is the clear nonplanarity of the diprotonated ligand. This result is significant because it demonstrates that the observed ruffling of Me$_2$BBZ is intrinsic to the ligand and is independent of bound metal (vide infra).

The structure of the corresponding Mn−Me$_2$BBZ complex was obtained as the dichloride salt, as is depicted in Figure 3 (see Tables 1 and 3). For consistency, atoms are labeled according to the same naming scheme as for the diprotonated Me$_2$BBZ ligand. The divalent manganese ion in the Mn−Me$_2$BBZ complex is five-coordinate and has a distorted square pyramidal geometry. The average bond distances are 2.12 Å

(36) Jonas, R.; Klockow, M.; Lues, I.; Prücher, H.; Schliep, H. J.; Wurziger, H. *Eur. J. Med. Chem.* **1993**, *28*, 129−140.

Table 1. Crystallographic Data for $[H_2(Me_2BBZ)](ClO_4)_2$ (**8**) and $[Mn(Me_2BBZ)Cl]Cl{\cdot}xH_2O$ (**9**)

	8	**9**
formula	$C_{30}H_{24}Cl_2N_6O_8$	$C_{30}H_{22}Cl_2MnN_6 + x(H_2O)$
fw	667.45	592.38[a]
temp, K	293	293
cryst syst	monoclinic	triclinic
space group	$P2_1/n$	$P\bar{1}$
a, Å	8.7086(2)	8.1128(3)
b, Å	28.8382(7)	13.3182(6)
c, Å	11.9403(3)	14.3727(6)
α, deg	90	67.527(1)
β, deg	100.147(1)	87.063(1)
γ, deg	90	83.148(1)
Z, formula unit	4	2
V, Å^3	2951.8(1)	1424.7(1)
d_{calcd}, g cm^{-3}	1.50	1.38[a]
μ_{calcd}, mm^{-1}	0.284	0.680[a]
no. data collected	18 805	16 307
no. unique data (all)	6743	7290
no. variable parameters	410	345
R_1,[b] wR2[c] (2σ)	0.097, 0.216	0.0515, 0.1007
R_1,[b] wR2[c] (all data)	0.169, 0.258	0.1283, 0.1203
gof on F^2 (all data)	1.039	0.899

[a] On the basis of the Mn complex only. [b] $R_1 = \sum||F_o| - |F_c||/\sum|F_o|$. [c] $wR2(F^2) = [\sum w(F_o^2 - F_c^2)^2/\sum w(F_o^2)^2]^{1/2}$, $w = 1/[\sigma^2(F_o^2) + (0.0841P)^2 + 7.8966P]$, where $P = (F_o^2 + 2F_c^2)/3$ for **8**, and $w = 1/[\sigma^2(F_o^2) + (0.0511P)^2 + 0.0000P]$, where $P = (F_o^2 + 2F_c^2)/3$ for **9**.

Table 2. Selected Bond Distances (Å) and Angles (deg) for $[H_2(Me_2BBZ)](ClO_4)_2$ (**8**)

N(1)−C(29)	1.342(6)	N(6)−C(16)	1.400(6)	C(13)−C(14)	1.470(7)
N(1)−C(1)	1.372(6)	N(6)−C(15)	1.470(6)	C(16)−C(17)	1.383(7)
N(2)−C(22)	1.270(6)	C(1)−C(2)	1.388(6)	C(16)−C(21)	1.386(7)
N(2)−C(23)	1.413(6)	C(1)−C(6)	1.414(7)	C(17)−C(18)	1.362(8)
N(3)−C(14)	1.334(6)	C(2)−C(3)	1.390(7)	C(18)−C(19)	1.390(8)
N(3)−C(21)	1.380(6)	C(3)−C(4)	1.384(8)	C(19)−C(20)	1.397(7)
N(4)−C(7)	1.262(6)	C(4)−C(5)	1.382(7)	C(20)−C(21)	1.392(6)
N(4)−C(8)	1.423(6)	C(5)−C(6)	1.384(7)	C(20)−C(22)	1.459(7)
N(5)−C(29)	1.344(6)	C(6)−C(7)	1.461(7)	C(23)−C(28)	1.396(7)
N(5)−C(2)	1.398(7)	C(8)−C(9)	1.394(7)	C(23)−C(24)	1.405(7)
N(5)−C(30)	1.477(6)	C(8)−C(13)	1.400(7)	C(27)−C(28)	1.414(7)
N(6)−C(14)	1.337(6)	C(12)−C(13)	1.391(7)	C(28)−C(29)	1.464(7)

C(29)−N(1)−C(1)	110.1(4)	C(1)−C(2)−C(3)	122.0(5)
C(22)−N(2)−C(23)	118.8(4)	C(1)−C(2)−N(5)	106.5(4)
C(14)−N(3)−C(21)	110.3(4)	C(3)−C(2)−N(5)	131.5(5)
C(7)−N(4)−C(8)	118.8(4)	C(4)−C(3)−C(2)	116.8(5)
C(29)−N(5)−C(2)	108.7(4)	C(5)−C(4)−C(3)	121.5(5)
C(29)−N(5)−C(30)	127.9(5)	C(4)−C(5)−C(6)	122.9(5)
C(2)−N(5)−C(30)	123.1(5)	C(5)−C(6)−C(1)	115.6(4)
C(14)−N(6)−C(16)	108.7(4)	C(5)−C(6)−C(7)	121.7(5)
C(14)−N(6)−C(15)	127.8(4)	C(1)−C(6)−C(7)	122.6(4)
C(16)−N(6)−C(15)	123.2(4)	N(4)−C(7)−C(6)	120.7(4)
N(1)−C(1)−C(2)	106.5(4)	C(9)−C(8)−C(13)	119.0(4)
N(1)−C(1)−C(6)	132.3(4)	C(9)−C(8)−N(4)	121.3(5)
C(2)−C(1)−C(6)	121.2(4)	C(13)−C(8)−N(4)	119.7(4)
C(12)−C(13)−C(8)	119.8(5)	C(19)−C(20)−C(22)	121.3(4)
C(12)−C(13)−C(14)	120.5(5)	N(3)−C(21)−C(16)	105.9(4)
C(8)−C(13)−C(14)	119.7(4)	N(3)−C(21)−C(20)	131.9(4)
N(3)−C(14)−N(6)	108.4(4)	C(16)−C(21)−C(20)	122.2(4)
N(3)−C(14)−C(13)	124.9(4)	N(2)−C(22)−C(20)	120.7(4)
N(6)−C(14)−C(13)	126.7(4)	C(28)−C(23)−C(24)	119.6(5)
C(17)−C(16)−C(21)	121.4(5)	C(28)−C(23)−N(2)	118.7(4)
C(17)−C(16)−N(6)	132.0(5)	C(24)−C(23)−N(2)	121.7(5)
C(21)−C(16)−N(6)	106.6(4)	C(23)−C(28)−C(27)	119.7(5)
C(18)−C(17)−C(16)	117.3(5)	C(23)−C(28)−C(29)	120.6(4)
C(17)−C(18)−C(19)	121.7(5)	C(27)−C(28)−C(29)	119.7(5)
C(18)−C(19)−C(20)	122.0(5)	N(1)−C(29)−N(5)	108.2(4)
C(21)−C(20)−C(19)	115.3(5)	N(1)−C(29)−C(28)	124.9(5)
C(21)−C(20)−C(22)	123.4(4)	N(5)−C(29)−C(28)	126.9(4)

for the Mn−N(benzimidazole) and 2.26 Å for the Mn−N(imine) nitrogens. One chloride serves as the axial ligand of the manganese ion with a Mn−Cl bond length of 2.319 Å. Like the diprotonated Me_2BBZ ligand, the Mn−Me_2BBZ complex is nonplanar.

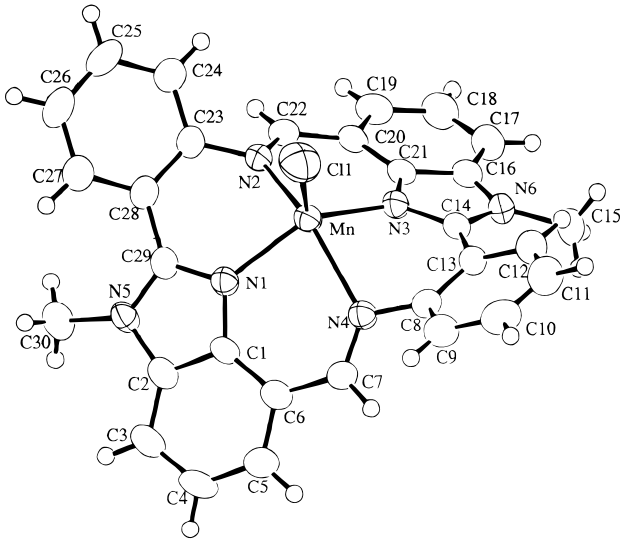

Figure 3. ORTEP diagram of $[Mn(Me_2BBZ)Cl]Cl$ (**9**).

The general features of the Mn−Me_2BBZ complex have similarity to manganese tetrapyrroles (porphyrins and phthalocyanines). Both manganese(II) porphyrins and bisbenzimidazoles favor a five-coordinate square pyramidal geometry and bind the metal around the equatorial plane. Moreover, the Mn−N(benzimidazole) and Mn−Cl distances of the Mn−Me_2BBZ complex are in the range of those of structurally characterized five-coordinate Mn(II) porphyrins, with an average 2.1 Å for Mn−N(porphyrin) bond distances and 2.37 Å for Mn−Cl(axial) distances.[37,38] The Mn(II)−N(imine) distances of the Mn−Me_2BBZ complex are slightly longer, however.

Similar comparison with the phthalocyanines is complicated by the fact that no five-coordinate Mn(II) phthalocyanines have been structurally characterized to date. Four-coordinate Mn(II) phthalocyanines, however, have been isolated and exhibit shorter Mn(II)−N(pyrrole) bond distances of 1.94 Å.[39,40] The smaller "central hole" size of phthalocyanines relative to porphyrins has been used to explain its shorter Mn−N bond lengths.[39] Although for different reasons, this issue is likely relevant to the Me_2BBZ ligand as well.

One structural feature that may be influenced by the size of the metal-binding pocket is the out-of-plane metal distance. In both Mn(II) porphyrins and the Mn−Me_2BBZ complex, the central Mn ion is significantly shifted away from the mean ligand plane. In the case of Mn(II) porphyrins, the distance of the Mn ion from the mean porphyrinato plane has been reported to be 0.56 Å for Mn(II)(TPP)(1-methylimidazole)[37,41] (TPP = *meso*-tetraphenylporphyrin) and 0.614 Å for Mn(II)(TPP)Cl.[38] In the present study, the Mn ion of the Mn−Me_2BBZ complex is shifted 0.796 Å from the mean plane of the four nitrogen ligands and 1.05 Å from the mean plane formed from the 22 atoms that are conserved between porphyrins and the Me_2BBZ

(37) Gonzalez, B.; Kouba, J.; Yee, S.; Reed, C. A.; Kirner, J. F.; Scheidt, R. *J. Am. Chem. Soc.* **1975**, *97*, 3247−3249.
(38) VanAtta, R. B.; Strouse, C. E.; Hanson, L. K.; Valentine, J. S. *J. Am. Chem. Soc.* **1987**, *109*, 1425−1434.
(39) Kirner, J. F.; Dow, W.; Scheidt, W. R. *Inorg. Chem.* **1976**, *15*, 1685−1690.
(40) Mason, R.; Williams, G. A. *J. Chem. Soc., Dalton Trans.* **1979**, 676−683.
(41) Kirner, J. F.; Reed, C. A.; Scheidt, W. R. *J. Am. Chem. Soc.* **1977**, *99*, 2557−2563.

Table 3. Selected Bond Distances (Å) and Angles (deg) for $[Mn(Me_2BBZ)Cl]Cl{\cdot}xH_2O$ (**9**)

Mn−N(3)	2.118(2)	Mn−N(2)	2.257(2)	Mn−Cl(1)	2.3186(10)
Mn−N(1)	2.127(2)	Mn−N(4)	2.277(2)		
N(1)−C(29)	1.339(3)	N(6)−C(16)	1.385(3)	C(13)−C(14)	1.479(4)
N(1)−C(1)	1.385(3)	N(6)−C(15)	1.458(3)	C(16)−C(21)	1.385(4)
N(2)−C(22)	1.289(3)	C(1)−C(2)	1.391(4)	C(16)−C(17)	1.395(4)
N(2)−C(23)	1.433(3)	C(1)−C(6)	1.412(4)	C(17)−C(18)	1.377(4)
N(3)−C(14)	1.342(3)	C(2)−C(3)	1.395(4)	C(18)−C(19)	1.382(4)
N(3)−C(21)	1.388(3)	C(3)−C(4)	1.371(4)	C(19)−C(20)	1.404(4)
N(4)−C(7)	1.280(3)	C(4)−C(5)	1.393(4)	C(20)−C(21)	1.404(4)
N(4)−C(8)	1.438(3)	C(5)−C(6)	1.397(4)	C(20)−C(22)	1.454(4)
N(5)−C(29)	1.365(3)	C(6)−C(7)	1.459(4)	C(23)−C(24)	1.386(4)
N(5)−C(2)	1.392(3)	C(8)−C(9)	1.389(4)	C(23)−C(28)	1.407(4)
N(5)−C(30)	1.466(3)	C(8)−C(13)	1.412(4)	C(27)−C(28)	1.394(4)
N(6)−C(14)	1.367(3)	C(12)−C(13)	1.376(4)	C(28)−C(29)	1.477(4)

N(3)−Mn−N(1)	128.88(9)	N(2)−Mn−N(4)	145.30(9)
N(3)−Mn−N(2)	84.81(8)	N(3)−Mn−Cl(1)	117.68(7)
N(1)−Mn−N(2)	80.55(8)	N(1)−Mn−Cl(1)	113.38(6)
N(3)−Mn−N(4)	79.65(8)	N(2)−Mn−Cl(1)	109.65(7)
N(1)−Mn−N(4)	85.39(8)	N(4)−Mn−Cl(1)	105.05(6)
C(29)−N(1)−C(1)	106.2(2)	C(22)−N(2)−C(23)	116.3(2)
C(29)−N(1)−Mn	127.7(2)	C(22)−N(2)−Mn	130.1(2)
C(1)−N(1)−Mn	125.8(2)	C(23)−N(2)−Mn	113.5(2)
C(14)−N(3)−C(21)	105.7(2)	C(13)−C(8)−N(4)	121.1(2)
C(14)−N(3)−Mn	127.4(2)	C(12)−C(13)−C(8)	118.7(3)
C(21)−N(3)−Mn	126.9(2)	C(12)−C(13)−C(14)	120.2(3)
C(7)−N(4)−C(8)	118.0(2)	C(8)−C(13)−C(14)	121.1(2)
C(7)−N(4)−Mn	129.6(2)	N(3)−C(14)−N(6)	111.3(2)
C(8)−N(4)−Mn	112.2(2)	N(3)−C(14)−C(13)	122.5(2)
C(29)−N(5)−C(2)	107.3(2)	N(6)−C(14)−C(13)	126.0(2)
C(29)−N(5)−C(30)	129.5(2)	C(21)−C(16)−N(6)	106.3(2)
C(2)−N(5)−C(30)	122.9(2)	C(21)−C(16)−C(17)	122.0(3)
C(14)−N(6)−C(16)	107.1(2)	N(6)−C(16)−C(17)	131.7(3)
C(14)−N(6)−C(15)	129.0(2)	C(18)−C(17)−C(16)	117.1(3)
C(16)−N(6)−C(15)	123.6(2)	C(17)−C(18)−C(19)	121.7(3)
N(1)−C(1)−C(2)	109.4(2)	C(18)−C(19)−C(20)	121.8(3)
N(1)−C(1)−C(6)	130.0(2)	C(19)−C(20)−C(21)	116.3(3)
C(2)−C(1)−C(6)	120.6(2)	C(19)−C(20)−C(22)	119.5(3)
C(1)−C(2)−N(5)	105.9(2)	C(21)−C(20)−C(22)	124.1(2)
C(1)−C(2)−C(3)	122.6(3)	C(16)−C(21)−N(3)	109.5(2)
N(5)−C(2)−C(3)	131.5(3)	C(16)−C(21)−C(20)	121.0(2)
C(4)−C(3)−C(2)	116.4(3)	N(3)−C(21)−C(20)	129.5(2)
C(3)−C(4)−C(5)	122.4(3)	N(2)−C(22)−C(20)	124.5(2)
C(4)−C(5)−C(6)	121.6(3)	C(24)−C(23)−C(28)	119.5(3)
C(5)−C(6)−C(1)	116.3(3)	C(24)−C(23)−N(2)	119.2(2)
C(5)−C(6)−C(7)	119.1(3)	C(28)−C(23)−N(2)	121.3(2)
C(1)−C(6)−C(7)	124.5(2)	C(27)−C(28)−C(23)	117.8(3)
N(4)−C(7)−C(6)	124.4(3)	C(27)−C(28)−C(29)	120.3(2)
C(9)−C(8)−C(13)	119.6(3)	C(23)−C(28)−C(29)	121.8(2)
C(9)−C(8)−N(4)	119.2(3)	N(1)−C(29)−N(5)	111.3(2)
N(1)−C(29)−C(28)	123.0(2)		
N(5)−C(29)−C(28)	125.7(2)		

ligand. These larger out-of-plane distances for the Me_2BBZ complex may be an indication of a smaller metal-binding pocket or could reflect the ability of the Me_2BBZ to twist and accommodate the requirements of the metal ion.

Crystal Packing in Mn−Me$_2$BBZ. Analysis of the crystal packing interactions in the Mn−Me_2BBZ crystals reveals another interesting consequence of the unusual Me_2BBZ ligand geometry. Because of the twist of the Me_2BBZ ligand and the fixed planarity of the phenyl and benzimidazole units, $[Mn(Me_2BBZ)Cl]^+$ molecules arrange themselves into two-dimensional layers comprised of alternating $[Mn(Me_2BBZ)Cl]^+$ atropisomers (Figure 4). In the crystal, each Mn−Me_2BBZ complex interacts with three other molecules of the opposite hand via π-stacking interactions (Figure 4). Two of the intermolecular π-stacking interactions involve benzimidazole rings of adjacent $[Mn(Me_2BBZ)Cl]^+$ molecules. These interactions are found on opposing sides of the Mn−Me_2BBZ complex such that if "L" represents one hand and "7" the other, then linear L·7·L·7·L·7 chains are formed along the direction of the benzimidazole stacking. The distance between stacked benzimidazole rings is 3.44 and 3.35 Å for the two distinct L·7 and 7·L stacking interactions, respectively. The third intermolecular interaction involves the phenyl rings of two $[Mn(Me_2BBZ)Cl]^+$ molecules located on different L·7·L·7·L·7 chains. The intermolecular distance between the phenyl rings here is 3.85 Å. Only one of the two phenyl rings of each $[Mn(Me_2BBZ)Cl]^+$ molecule is involved in intermolecular interactions. The other phenyl ring forms one side of an intermolecular channel.

Because the phenyl and benzimidazole stacking interactions within the Mn−Me_2BBZ crystal are directed in perpendicular directions, they generate an unusual lattice comprised of two-dimensional "staircase" layers. These layers lie in the plane generate by the *b* and *c* axes of the crystal, termed the *A* plane. The three-dimensional lattice is generated by translation of these "staircase" layers by one unit cell length along the *a* axis, resulting in stacks of "staircase" layers each of which is slightly horizontally shifted from the layer above and below.

Because of the low symmetry of the crystal, molecules of the same hand lie above one another along the *a* axis. This results in the formation of columnar chains of $[Mn(Me_2BBZ)Cl]^+$ units directed in the $+a$ and $-a$ directions. The axial ligand in each chain is directed along the *a* axis as well. Importantly, as in porphyrins, covalent interactions between bisbenzimidazole units must occur through their axial ligands. Hence, this arrangement offers the possibility of generating covalent donor−acceptor chains along the *a* axis.

Perhaps of greater significance is the fact that the extensive π-stacking interactions within the Mn−Me_2BBZ crystal promote greater cohesion of the molecular bisbenzimidazole units than are typically found in crystals of metalloporphyrins or phthalocyanines. Within each layer, the intermolecular Mn−Mn distances are 8.997 and 8.971 Å through the two 7·L and L·7 benzimidazole-stacking interactions, respectively, and 11.400 Å through the phenyl-stacking interaction. The distance between layers is the length of the *a* axis or 8.113 Å.

These intermolecular interactions could be of particular importance in the design and synthesis of materials that require cooperative electronic and/or magnetic couplings. For example, in the molecular magnet formed from linear chains of $[MnTPP]^+[TCNE]^-$ donor−acceptor pairs, ferro- or ferrimagnetic interchain coupling is a requirement for observed ferrimagnetic behavior. In crystals of $[MnTPP]^+[TCNE]^-$, the intermolecular Mn−Mn separations across the chains are 13.269 and 14.932 Å for atoms in the same plane, while the out-of registry Mn−Mn separations are 11.006, 11.823, and 13.838 Å. Because the strength of the electronic and magnetic coupling is distance-dependent, the shorter Mn−Mn interchain distances in Mn−Me_2BBZ crystals compared to corresponding porphyrin and phthalocyanine crystals suggest that the Mn−Me_2BBZ "staircase" layer could be a favorable structural motif for the design of novel materials. Studies designed to take advantage of these observations are currently underway.

Optical Spectra. The optical spectrum of the diprotonated Me_2BBZ ligand exhibits strong absorptions in the ultraviolet region (Figure 5). Major bands are found at 235 ($\epsilon = 3.17 \times 10^4$ M cm^{-1}), 270 ($\epsilon = 3.14 \times 10^4$ M cm^{-1}), and 302 nm ($\epsilon = 2.84 \times 10^4$ M cm^{-1}). The Mn−Me_2BBZ complex exhibits similar transitions, but energies appear red-shifted (Figure 5). Two broad bands centered at 243 nm ($\epsilon = 3.50 \times 10^4$ M cm^{-1}) and 328 nm ($\epsilon = 4.78 \times 10^4$ M cm^{-1}) are observed.

For comparison, porphyrins typically exhibit a strong Soret absorption around 400 nm and less intense Q-bands centered

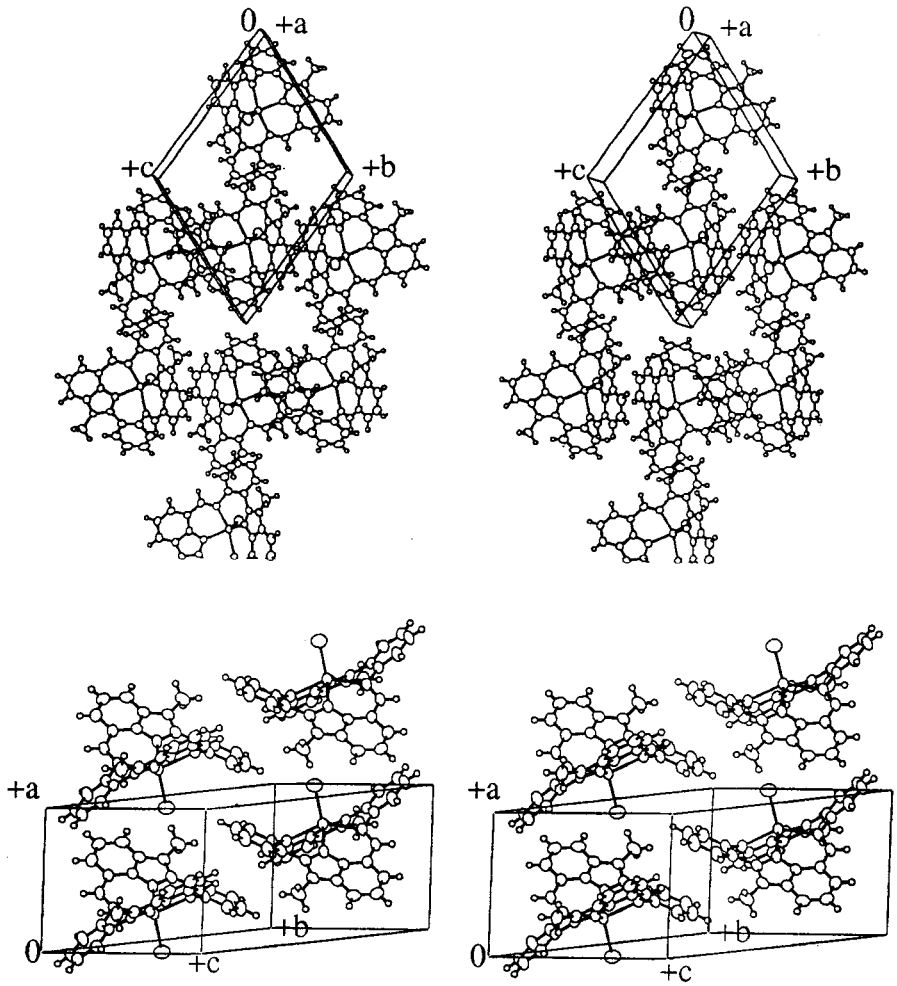

Figure 4. (top) Stereoview of the two-dimensional "staircase" layer. The L·7·L·7·L·7 benzimidazole stacking interactions are aligned horizontally. The phenyl−phenyl stacking interactions are aligned vertically. The channel lies at the origin. (bottom) Perpendicular view showing arrays of aligned atropisomers. Binding of ligands between successive molecules could potentially lead to donor−acceptor chains.

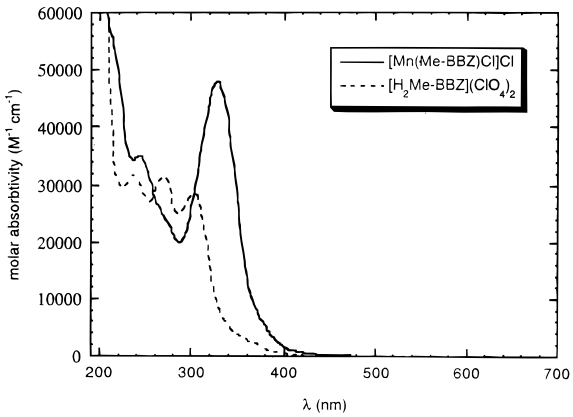

Figure 5. Optical spectrum of the diprotonated $[H_2(Me_2BBZ)](ClO_4)_2$ ligand and the $[Mn(Me_2BBZ)Cl]Cl$ complex.

near 600 nm.[42−44] Phthalocyanines behave similarly. Strong Soret and Q-band absorptions are observed in the vicinity of 320−370 and 670−690 nm, respectively.[45,46] The similarity of these optical energies and extinction coefficients among bisbenzimidazoles and classical tetrapyrroles suggests that the spectra of the Me_2BBZ ligand and Mn−Me_2BBZ complex likely result from $\pi-\pi^*$ transitions as well. Unlike porphyrins and phthalocyanines, however, bisbenzimidazoles do not appear to exhibit the low-energy Q-band absorption. One interesting consequence of the absence of a Q-band is the lack of significant absorptions in the visible spectrum (from 500 to 900 nm). This outcome could have important ramifications for the practical use of bisbenzimidazoles in nonoptical materials, particularly those applications where visible absorptions would be detrimental.

EPR Spectroscopy of the Mn−Me_2BBZ Complex. The EPR spectrum of the frozen Mn−Me_2BBZ complex (Figure 6) shows six sharp lines centered at $g = 2$ characteristic of a high-spin Mn(II) ion with a small zero-field splitting. As expected, only the transitions within the $m_s = -1/2 \leftrightarrow m_s = +1/2$ manifold are observed. The observed nuclear hyperfine splitting is typical of a high-spin manganese ion ($|A| = 95 \pm 1$ G).

Above 173 K, the hyperfine components are broadened because of relaxation effects. However, at temperatures lower than 173 K, the spectrum sharpens to reveal lines of lower intensity between the major transitions that are resolved. These

(42) Falk, J. E. *Porphyrins and Metalloporphyrins: Their General, Physical and Coordination Chemistry, and Laboratory Methods*; Elsevier Publishing Company: Amsterdam, 1964.
(43) Gouterman, M. *Optical Spectra and Electronic Structure*; Dolphin, D., Ed.; Academic Press: New York, 1977; Vol. III, Part A, pp 1−165.
(44) Loew, G. H. *Theoretical Investigations of Iron Porphyrins*; Lever, A. B. P., Gray, H. B., Eds.; Addison-Wesley Publishing Company: Reading, MA, 1983; pp 1−87.
(45) Moser, F. H.; Thomas, A. L. *The Phthalocyanines: Properties*; CRC Press: Boca Raton, FL, 1983; Vol. 1.
(46) McKeown, N. B. *Phthalocyanine Materials*; Cambridge University Press: Cambridge, U.K., 1998.

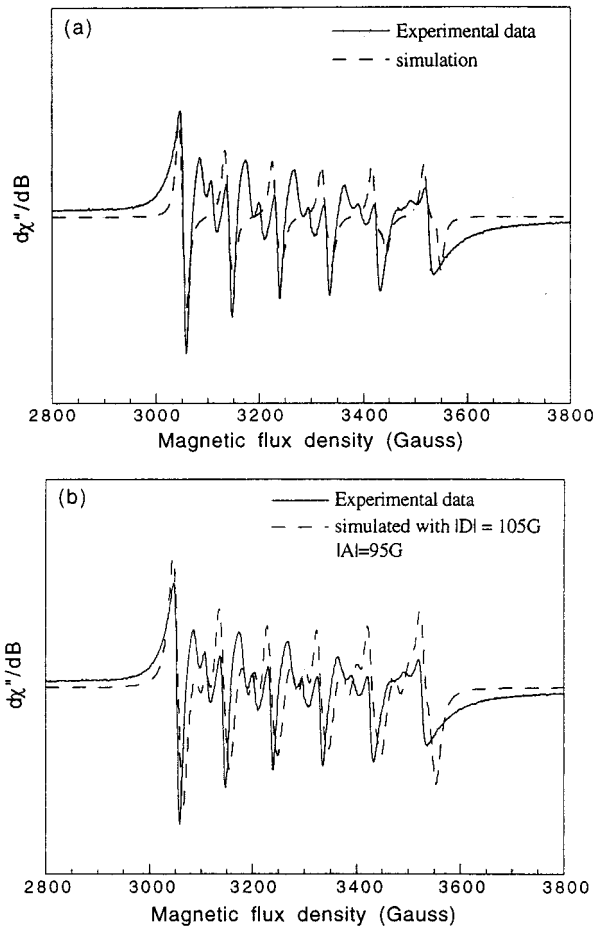

Figure 6. EPR spectra of [Mn(Me$_2$BBZ)Cl]Cl (**9**): (a) experimental data (solid line) and calculated spectrum (dashed line) simulated without inclusion of second-order effects on transition probabilities and forbidden transitions with $|A| = 95$ G and $|D| = 105$ G. (b) Experimental data (solid line) and fully simulated spectra (dashed line) computed with the same $|A|$ and $|D|$ values as for (a).

smaller transitions are in the correct field positions to be assigned to the $\Delta m_s = +1$, $\Delta m_I = \pm 1$ forbidden transitions, and all 10 expected transitions are discerned. These spectral features are indicative of a nearly cubic environment for the high-spin Mn(II) ion, which is consistent with the out-of-plane distortion of the metal from the mean ligand plane.

The value of D, the axial splitting parameter, may be estimated from the intensity of the transitions.[47] Another method involves analysis of the intensity ratios of the allowed transitions.[48] An upper limit of 150−200 G or 0.015−0.02 cm^{-1} was estimated for D by this procedure. A more reliable determination was obtained by spectral simulation using the program EPR-NMR (Department of Chemistry, University of Saskatchewan, Canada). In this manner, the observed spectrum could be simulated to best-fit both the positions and intensities of the forbidden lines. We obtained $|A| = 95$ G and $D = 0.01$ cm^{-1} from these simulations. The calculated EPR spectrum using these values shows good agreement with the experimental data (Figure 6).

Magnetic Susceptibility Measurements of the Mn−Me$_2$BBZ Complex. In light of the unusual molecular packing within the Mn−Me$_2$BBZ crystal, temperature-dependent magnetic susceptibility measurements were performed to determine the extent of any sizable intermolecular magnetic interaction. The experimental data are shown in Figure 7. At room temperature, $S \approx 2.5$ and $\mu_{eff} = 5.96$, consistent with a high-spin Mn(II) ion. The Curie constant (C) and Weiss correction (θ) obtained are 4.47 and −0.97, respectively. The negative θ provides a measure of the zero-field splitting (D) and the near-neighbor superexchange interactions (J).

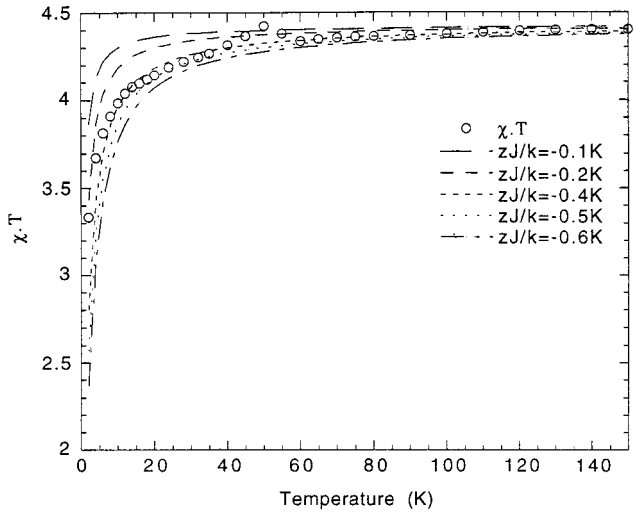

Figure 7. Comparison of the magnetic susceptibility data (open circle) and the calculated susceptibility curves determined using eqs 1−9 with various zJ/k values (−0.1 to about −0.6 K).

Following earlier work, the susceptibility data were fitted using a model proposed by Watanabe[49] and McElearney et al.[50] in which the intermolecular exchange interactions were treated as a perturbing molecular field. First, we write the total spin Hamiltonian of a single ion as

$$H = g\beta S_z H - DS_z^2 \tag{1}$$

The energy levels for the ion for different orientations of the magnetic field along the molecular x, y, z axes can be readily calculated. Using these results, we obtain the following expressions for the anisotropic magnetic susceptibility:

$$\chi_{\parallel} = \frac{2Ng^2\mu_B^2}{kT}\frac{1 + 9\,e^{-2D/(kT)} + 25\,e^{-6D/(kT)}}{1 + e^{-2D/(kT)} + e^{-6D/(kT)}} \tag{2}$$

$$\chi_{\perp} = \frac{2Ng^2\mu_B^2}{kT}\frac{9 + \frac{8kT}{D} - \frac{11kT}{2D}e^{-2D/(kT)} - \frac{5kT}{D}e^{-6D/(kT)}}{1 + e^{-2D/(kT)} + e^{-6D/(kT)}} \tag{3}$$

For high-spin Mn(II), the molecular g values are isotropic. The molecular exchange field is then introduced by adding an exchange term into the spin Hamiltonian. In the mean field approximation $2\sum_j J_{ij}S_i \cdot S_j$ is replaced by $A \cdot \mathbf{S}\langle\mathbf{S}\rangle$, the thermal equilibrium approximation and where A is the molecular field coefficient. The relation between $A \cdot \mathbf{S}\langle\mathbf{S}\rangle$ and $2\sum_j J_{ij}S_i \cdot S_j$ is

$$-2\sum_j J_{ij}S_i \cdot S_j \approx -2zJ\mathbf{S} \cdot \langle\mathbf{S}\rangle = A\mathbf{S} \cdot \langle\mathbf{S}\rangle \tag{4}$$

where $-2zJ = A$ and z and J denote the number of nearest neighbors and the exchange integral, respectively. The molecular

(47) Kuska, H. A.; Rogers, M. T. *Radical Ions*; Kaiser, E. T., Kevan, L., Eds.; Wiley-Interscience: New York, 1968; pp 638−666.
(48) Allen, B. T. *J. Chem. Phys.* **1965**, *43*, 3820.
(49) Watanabe, T. *J. Phys. Soc. Jpn.* **1962**, *17*, 1856−1864.
(50) McElearney, J. N.; Losee, D. B.; Merchant, S.; Carlin, R. L. *Phys. Rev.* **1973**, *B7*, 3314−3324.

exchange field is then

$$H' = \frac{2zJ}{Ng^2\mu_B{}^2}\chi_i' H_i, \quad i = \parallel, \perp \tag{5}$$

where χ_i' is the exchange-corrected susceptibility actually measured and where H_i denotes the external field. The resulting exchange fields are assumed to be collinear.

Thus, there is an additional field turned on in the presence of the applied or measuring field. Accordingly,

$$M_i = \chi_i(H_i + H_i') \tag{6}$$

By definition the measured susceptibility is given by

$$\chi_i' = \lim_{H_i \to 0} \frac{M_i}{H_i} \tag{7}$$

The exchange-corrected susceptibility is then given by [combining eqs (5−7)]

$$\chi_i' = \frac{\chi_i}{1 - \left(\frac{2zJ}{Ng^2\mu_B{}^2}\right)\chi_i} \tag{8}$$

For powder samples, we obtain

$$\chi_{\text{powder}} = (2\chi_\perp' + \chi_\parallel')/3 \tag{9}$$

Figure 7 shows the fit to the experimental data in the form of $\chi_{\text{powder}}T$ vs temperature plots. For the best fit, $J/k = 0.4$ K (0.278 cm^{-1}) and $D/k = 0.01$ K (0.007 cm^{-1}). From these two results, it is clear that the value of J has a more significant effect on the susceptibility data than the zero-field splitting. In fact, a wide range of D values fit the data fairly well (0.01−1 K), indicating that the zero-field terms cannot account for the observed magnetic features. Ginsberg et al.[51] have noted a similar zero-field-independent magnetic susceptibility for a dimeric system with intramolecular antiferromagnetic exchange interaction.

From the sign of J, the exchange interaction is also antiferromagnetic in the present case. While the weak antiferromagnetic coupling determined from these measurements would not be favorable toward the preparation of ferrimagnetic materials, these data do support the notion that the "staircase" motif can mediate weak electronic and magnetic interactions. The sign of these exchange-coupled interactions (ferro- or antiferromagnetic) could be dependent on subtle alterations at the metal center (i.e., metal species, extent of ruffling, symmetry of the metal environment). Further studies of other related complexes should help to elucidate the factors that modulate the nature of these intermolecular couplings.

Electrochemical Studies. While cyclic voltammetry measurements of the Me_2BBZ ligand provide no evidence for ligand-based redox activity, similar measurements of the Mn−Me_2BBZ complex reveal a quasi-reversible redox wave for the bound manganese ion ($\Delta E_{\text{peak}} = 66$ mV). A Mn(II)/Mn(III) redox couple centered at 0.53 V vs ferrocene/ferrocenium (0.99 V vs SCE) is observed in acetonitrile.

Manganese(II) porphyrins also exhibit metal-centered oxidations with Mn(II)/Mn(III) and Mn(III)/Mn(IV) redox potentials of −0.2 and ∼1.0 V vs SCE, respectively.[52,53] In Mn(II) phthalocyanines, however, while the potential of the Mn(II)/Mn(III) phthalocyanine couple is −0.1 V vs SCE, the second oxidative wave centered at 0.86 V vs SCE originates from a reversible ligand oxidation.[54] Comparison of these redox potentials suggests that porphyrins and phthalocyanines are better at stabilizing higher oxidation states, the origin of these different redox properties being the difference in the inherent charges of the tetrapyrrole (dianionic) and bisbenzimidazole (neutral) ligands. It will be interesting to learn how these redox differences are reflected in the catalytic chemistry of metal bisbenzimidazole complexes.

Discussion

Nonplanarity of Bisbenzimidazole Complexes. One of the most important features of the Me_2BBZ ligand is its intrinsic nonplanarity. Analyses of the diprotonated Me_2BBZ and Mn−Me_2BBZ structures suggest that the driving force for this ruffling stems from two types of steric interactions: (1) interactions between the protons of the Schiff base with those on the phenyl ring (the C(7)−H hydrogen with the C(9)−H hydrogen, and the C(22)−H hydrogen with the C(24)−H hydrogen); (2) interactions within each phenylbenzimidazole group between the methyl substituent and the neighboring phenyl ring (the C(15) methyl group with the C(12)−H hydrogen, and the C(30) methyl group with the C(27)−H hydrogen (Figures 3 and 4). In addition, geometric constraints require that specific atoms within each phenylbenzimidazole unit be collinear (atoms C(29), C(28), and C(25) being one set and atoms C(10), C(13), and C(14) being the other). The net effect of these steric interactions and geometric constraints is a significantly twisted ligand with two distinct and well-defined ligand planes.

The extent of nonplanarity for different Me_2BBZ complexes can be evaluated by simply determining the out-of-plane distances of each ligand atom from the mean plane of the four liganding nitrogen atoms. These out-of-plane distances have been calculated for both the diprotonated Me_2BBZ ligand and Mn−Me_2BBZ complex and are shown in Figure 8. The relative shifts (both above and below the plane) for the atoms in common in both complexes reveal that the diprotonated Me_2BBZ ligand is more nonplanar, providing further evidence that bisbenzimidazole ruffling is an inherent feature of the ligand.

While a comparison of the nonplanarities of bisbenzimidazoles and porphyrins is more difficult, an analysis of their general features can be undertaken. In porphyrins, the displacement of the C_m and C_b carbons is commonly used to estimate their nonplanar distortions.[55] For the Me_2BBZ ligand and Mn−Me_2BBZ complex, the C_m atoms correspond to C(6), C(13), C(20), and C(28), while the C_b atoms correspond to N(5), C(2), C(9), N(6), C(16), and C(24). The maximum C_m and C_b displacements for several Mn(II) porphyrins and the two Me_2BBZ structures reported in this work are tabulated in Table 4. These comparisons indicate that the ligand out-of-plane distances for our Me_2BBZ compounds are significantly larger than for porphyrins.

(51) Ginsberg, A. P.; Martin, R. L.; Brookes, R. W.; Sherwood, R. C. *Inorg. Chem.* **1972**, *11*, 2884−2889.
(52) Guilard, R.; Perie, K.; Barbe, J.-M.; Nurco, D. J.; Smith, K. M.; Caemelbecke, E. V.; Kadish, K. M. *Inorg. Chem.* **1998**, *37*, 973−981.
(53) Jeon, S.; Bruice, T. C. *Inorg. Chem.* **1992**, *31*, 4843−4848.
(54) Lever, A. B. P.; Minor, P. C.; Wilshire, J. P. *Inorg. Chem.* **1981**, *20*, 2550−2553.
(55) Scheidt, W. R.; Lee, Y. J. *Struct. Bonding* **1987**, *64*, 1−70.
(56) Kirner, J. F.; Scheidt, W. R. *Inorg. Chem.* **1975**, *14*, 2081−2086.
(57) Hill, C. L.; Williamson, M. M. *Inorg. Chem.* **1985**, *24*, 3024−3030.
(58) Scheidt, W. R.; Hatano, K.; Rupprecht, G. A.; Piciulo, P. L. *Inorg. Chem.* **1979**, *18*, 292−299.
(59) Navaza, A.; de Rango, C.; Charpin, P. *Acta Crystallogr.* **1983**, *C39*, 1625−1628.

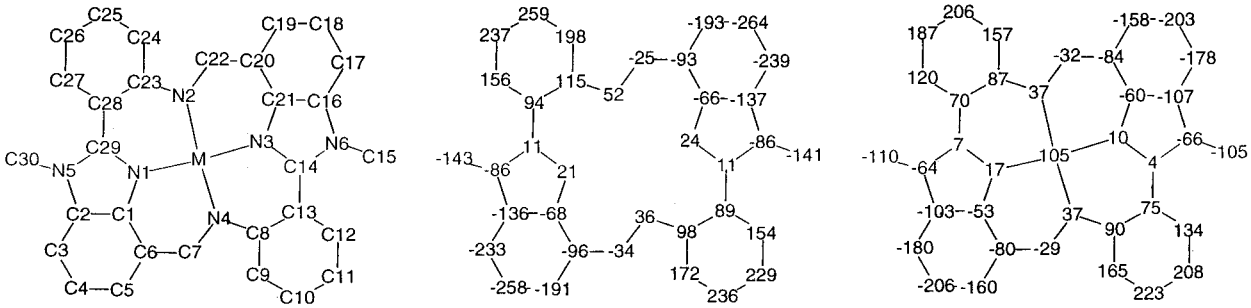

Figure 8. Perpendicular displacement of each atom, in units of 0.01 Å, from the mean plane of the four nitrogen atoms that bind metal ions: labeling scheme (left); $[H_2(Me_2BBZ)](ClO_4)_2$ (**8**) (center); $[Mn(Me_2BBZ)Cl]Cl$ (**9**) (right).

Table 4. Comparison of the Displacements of the C_m and C_b Atoms in Representative Nonplanar Porphyrins and the Displacements of the Corresponding Atoms in the Two Bisbenzimidazole Structures

compound	distortion mode	average absolute displacement		ref
		C_m [a]	C_b [a]	
$[H_2(Me_2BBZ)](ClO_4)_2$	twist	93	136	
$[Mn(Me_2BBZ)Cl]Cl$	twist	77	110	
Mn(TPP)(1-MeIm)[b]	dom	5	18	41
[Mn(TPP)(Py)Cl][b]	ruf	30	26	56
$[Mn(TPP)(2,6\text{-LutNO})_2]ClO_4$[b]	ruf	44	17	57
Mn(TTP)(NO)[c]	sad	16	35	58
H_4TPP^{2+} [b]	sad	6	90	59

[a] Value in Å × 10^2. [b] TPP: dianion of 5,10,15,20-tetraphenylporphyrin. 1-MeIm: 1-methylimidazole. 2,6-LutNO: 2,6-dimethylpyridine-*N*-oxide. [c] TTP: dianion of 5,10,15,20-tetra-*p*-tolylporphyrin.

Because of their significant nonplanarities and their intrinsically lower C2 symmetry, bisbenzimidazoles appear to exist as two distinct atropisomers. These atropisomers can be distinguished by the orientation of the phenylbenzimidazole units relative to the nonplanar distortion. In light of the steric interactions described above, these atropisomers would be expected to have high barriers to interconversion, particularly in the case of the metalated forms (vide infra). This result is significant because the ligand nonplanar twist generates a chiral pocket whose hand is dependent on the hand of the atropisomer. Hence, there is potential that each atropisomer, when separated, could be used to promote chiral recognition or asymmetric catalysis at the metal center. Studies to test these ideas are presently underway.

Summary and Conclusions

We have synthesized a new class of nonplanar porphyrin analogue as the first step toward the development of novel catalysts and molecular materials. The structures of the diprotonated Me_2BBZ ligand and the $[Mn(Me_2BBZ)Cl]^+$ complex reveal significant ruffling that is distinct from the classical modes exhibited by porphyrins. The low symmetry of the ligand and its inherent nonplanarity lead to two distinct atropisomers that in principle could be separated and used to prepare chiral shift reagents and catalysts. Of equal interest is the unusual crystal-packing interactions exhibited by the Mn−Me_2BBZ complex. The extensive π-stacking and compact metal−metal distances suggest that materials based on bisbenzimidazoles have potential for greater three-dimensional magnetic and electronic couplings than those found in typical porphyrin and phthalocyanine materials. Another major difference between porphyrins and bisbenzimidazoles is in their charge and electronic structures. These differences could provide bisbenzimidazole complexes with distinct properties that could lead to their use in new applications. Indeed, recent studies describing the use of the unique properties of bisbenzimidazoles in sensing and catalysis will be reported in due course.

Acknowledgment. We are grateful to the College of Arts and Sciences Instrumentation Center at the University of Toledo for access to the SMART 1K CCD diffractometer. The temperature-dependent magnetization data were collected at the Beckman Institute SQUID facility at the California Institute of Technology. We thank Joshua A. Maurer for his assistance in the SQUID data collection and Dr. Sunney I. Chan of the Department of Chemistry at California Institute of Technology for his insights into the fitting of the EPR and magnetic data. This work was partially supported by funds from The Ohio State University and the Hermann Frasch Foundation (Grant 416-HF97 to M.K.C.) D.H.J. was supported by funds from the Petroleum Research Foundation (to M.K.C.).

Supporting Information Available: Cyclic voltamogram of the Mn−Me_2BBZ complex and listings of the additional crystallographic data (coordinates and anisotropic thermal parameters). This material is available free of charge via the Internet at http://pubs.acs.org.

IC991322A